JCTC Journal of Chemical Theory and Computation

Molecular Dynamics and Room Temperature Vibrational Properties of Deprotonated Phosphorylated Serine

A. Cimas,[†] P. Maitre,[‡] G. Ohanessian,[§] and M.-P. Gaigeot*,[†]

Laboratoire Analyse et Modélisation pour la Biologie et l'Environnement, UMR8587 CNRS, Université d'Evry val d'Essonne, boulevard F. Mitterrand, Bat. Maupertuis, 91025 Evry Cedex, France, Laboratoire de Chimie Physique, Université Paris Sud 11, UMR8000 CNRS, Faculté des sciences, bâtiment 350, 91405 Orsay Cedex, France, and Laboratoire des Mécanismes réactionnels, Département de Chimie, Ecole Polytechnique, CNRS, 91128 Palaiseau Cedex, France

Received April 13, 2009

Abstract: The local structure of phosphorylated residues in peptides and proteins may have a decisive role on their functional properties. Recent IRMPD experiments have started to provide spectroscopic signatures of such structural details; however, a proper modeling of these signatures beyond the harmonic approximation, taking into account temperature and entropic effects, is still lacking. In order to bridge this gap, DFT-based Car−Parrinello molecular dynamics simulations have been carried out for the first time on a phosphorylated amino acid, gaseous deprotonated phosphoserine. It is found that all vibrational signatures are successfully reproduced, and new deconvolution techniques enable the assignment of the vibrational spectrum directly from the dynamics results and the comparison of vibrational modes at several temperatures. The lowest energy structure is found to involve a strong hydrogen bond between the deprotonated phosphate and the acid with relatively small free energy barriers to proton transfer; however, we find that proton shuttling between the two sites does not occur frequently. Anharmonicities turn out to be important to reproduce the frequencies and shapes of several experimental bands. Comparison of room temperature and 13 K, effectively harmonic dynamics, allows insight to be obtained into vibrational anharmonicities. In particular, a significant blue-shift and broadening of the C=O stretching frequency from 13 to 300 K can be ascribed to intrinsic anharmonicity rather than to anharmonic coupling to other modes. On the other hand, significant couplings are found for the stretching motions of the hydrogen bonded P−O bond and of the free P−OH bond, mainly with modes within the phosphate group.

1. Introduction

Reversible protein phosphorylation of the side chain alcohol group of serine (S), threonine (T), or tyrosine (Y) residues, is a very common post-translational modification (PTM) of proteins. It has a strong impact on protein function, as it influences metabolic pathways, membrane transport, gene transcription, etc.[1,2] The impact of phosphorylation on protein function is at least in some cases related to the conformational changes it induces.[3] It is thus of great interest to unravel the mechanism by which a single phosphorylation may significantly alter the structure of a macromolecule. Studies on peptides have revealed that phosphorylation can promote high helical content.[4] It has been recognized in several cases that the presence of nearby arginine (R) residues is likely to lead to strong hydrogen bonding between the negatively charged phosphate and the positively charged guanidinium of R.[3] Small models can therefore be of high value to quantify such individual interactions.[5]

* Corresponding author phone: +33-1-69470140; e-mail: mgaigeot@univ-evry.fr.

[†] Université d'Evry val d'Essonne.

[‡] Université Paris Sud 11.

[§] Ecole Polytechnique.

10.1021/ct900179d CCC: $40.75
Published on Web 08/13/2009

Phosphate groups are expected to have rather recognizable vibrational signatures;[6] therefore, IR spectroscopy is in principle a valuable tool to identify phosphates and their environment. In particular, IR spectroscopy of organic molecules is known to be highly sensitive to hydrogen bonding, a feature that makes this technique very appealing for structural characterization of phosphorylation. In previous work, we have shown that the recently developed InfraRed Multiple Photon Dissociation (IRMPD) spectroscopic technique can be used to detect the occurrence of phosphorylation in amino acids and peptides in the gas phase.

IRMPD is carried out by irradiating gaseous ions trapped in high vacuum cells of mass spectrometers with IR photons.[7−10] Because the number density of gaseous ions is necessarily small, absorption spectroscopy cannot be carried out. The photons are used to generate ion fragmentation, which is efficiently monitored with the high sensitivity of mass spectrometers. The fragmentation ratio as a function of photon energy generates an IR action spectrum. This technique requires high laser power and wide tunability, which are made available in the 200−2000 cm^{-1} region by free electron lasers (FEL).[7−10] IRMPD has the potential for distinguishing between isomers, and also between conformers, although the latter can be much more difficult. This new spectroscopic tool has already found many applications, including the structural characterization of small biological molecules such as peptides.[11−23]

In a previous paper, we obtained the IRMPD signatures of the three protonated, phosphorylated amino acids: phospho-serine ($[pS+H]^+$), phospho-threonine ($[pT+H]^+$), and phospho-tyrosine ($[pY+H]^+$).[24] The results indicated that phosphate specific bands exist as expected and that they are easily detectable in IRMPD conditions, in the vibrational range accessible with a FEL. Detailed band assignment based on quantum chemical calculations established that some features were common to all three species, while others were specific. Furthermore, a second distinction was established, in which it is the hydrogen bonding capability of the environment that is distinctive. This conclusion was confirmed by a subsequent study of the phosphorylated dipeptide $[GpY+H]^+$, showing the potential of the method.[25] The proof of principle for extension to larger biomolecules was given on a 12-residue fragment of the protein stathmin.[24] It is clear however that the most likely form of phosphates at physiological pH is deprotonated, either singly or doubly. We have therefore initiated a research program in which we generate and interpret the IRMPD spectra of deprotonated phosphorylated amino acids[26] and peptides.

Since IRMPD spectroscopy is a relatively new technique, extensive molecular modeling is required to interpret the bands. This has been done with success in the past with harmonic calculations (see, e.g. refs 11−23 for applications to peptides), i.e. optimizing the geometry of several possible structures for each species and generating harmonic vibrational spectra at the optimized geometries. A match between experimental and calculated IR signatures is subsequently sought to identify populated isomers and/or conformers. However modeling of band breadth has not been yet tackled, and there are a number of cases for which discrepancies between experimental and computed frequencies remain unexplained.

Because IRMPD experiments are often carried out at room temperature, a theoretical approach closer to the experimental conditions and applied in the present work consists in simulating the dynamical behavior of the molecule through molecular dynamics (MD) simulations conducted at the average experimental temperature, for instance through DFT-based Car−Parrinello MD (CPMD),[27] and calculating the IR spectrum directly from the dynamics. MD is essential for including temperature, conformational dynamics, in particular the interconversion between different conformers[28] or isomers such as those connected by proton transfers,[12,14] with the advantage that entropic effects are directly taken into account.

IR spectra calculations through MD simulations are based on a dipole time correlation function.[29] Within the past few years, we have shown that DFT-based MD is the proper tool for the calculation of IR spectra of DNA and peptide building blocks, in the gas phase or immersed in liquid water,[12,14,28,30−32] at room temperature. We have in particular demonstrated the role of conformational dynamics at room temperature in the interpretation of finite temperature spectroscopy of peptides,[28] which is relevant for IRMPD.

The main advantage of IR spectra calculations through finite temperature MD over static calculations is that all anharmonic effects are naturally described. This is to be opposed to the two successive harmonic approximations usually adopted for the determination of IR spectra from static *ab initio* calculations, i.e. the harmonic approximation of the potential energy surface at the optimized geometries and the electrical harmonic approximation for the transition dipole moments. Both approximations are relaxed in *ab initio* molecular dynamics, simply because they are not needed. In fact, the finite temperature dynamics takes place on all accessible parts of the potential energy surface (be they harmonic or anharmonic), provided that time propagation is long enough. As the calculation of IR spectra with molecular dynamics is related only to the time-dependent dipole moment of the molecule, it does not require any harmonic expansion of the transition dipole moments. Therefore, if the dipole moments and their fluctuations are accurately calculated along the trajectory, the resulting IR spectrum should be reliable too. The quality of the potential energy surface is entirely contained in the force field, calculated at the DFT/BLYP level in the present work, as in our previous investigations.[12,14,28,30−32] The very good reproduction of the relative positions (and intensities, when they are directly comparable to experiment[31,32]) of the different active bands in our previous works indicates that this level of theory is satisfactory, at least on weakly interacting floppy peptide building blocks (gas phase or immersed in liquid water). The B3LYP hybrid functional has been recently implemented in the CPMD[33] and CP2K MD packages,[34] but the CPU cost is reported to be ∼40−100 times larger than that of a GGA functional MD. Considering our previous results together with the extra-CPU cost for a hybrid DFT-based MD, we chose to keep to local BLYP MD simulations in the present work. New functionals have recently been implemented to

Table 1. Relative Energy Values (kcal/mol) between the Optimized Configurations of $[pSer\text{-}H]^-$ [b]

	B3LYP/all electron						BLYP/all electron							
	6-31+G(d)		6-311++G(d,p)		aug-cc-pVTZ		6-31+G(d)		6-311++G(d,p)		aug-cc-pVTZ		CPMD/BLYP	
isomer	without ZPE	including ZPE	without ZPE	including ZPE	without ZPE	including ZPE	without ZPE	including ZPE	without ZPE	including ZPE	without ZPE	including ZPE	90 Ry	110 Ry
pSer-H_1	0.00	0.00	0.00	0.00	0.00	0.00	0.00	0.00	0.00	0.00	0.00	0.0	0.00	0.00
pSer-H_2	1.46	0.64	1.75	0.94	1.19	0.59	1.30	0.47	1.55	0.75	1.03	0.47	0.84	0.92
pSer-H_3	3.89	3.71	5.69	5.38	-	-	2.54	2.37	4.18	3.91	4.59[a]	-	4.45	4.42
pSer-H_4	3.94	3.69	5.79	5.38	-	-	2.60	2.37	4.31	3.94	4.74[a]	-	4.46	4.44
pSer-H_5	11.89	10.80	-	-	-	-	11.45	10.47	-	-	-	-	10.75	10.71
pSer-H_6	11.89	10.91	-	-	-	-	10.92	10.02	-	-	-	-	10.93	10.92
pSer-H_7	11.89	11.05	-	-	-	-	11.42	10.67	-	-	-	-	11.02	10.99
pSer-H_8	13.76	13.26	-	-	-	-	13.57	13.03	-	-	-	-	13.73	13.71

[a] Single points over the optimized BLYP/6-31+G(d) geometries. [b] B3LYP and BLYP calculations refer to all electron geometry optimizations performed with the Gaussian03 package. CPMD refers to DFT/BLYP/pseudopotential single point calculations performed with a plane-wave basis set of 90 or 110 Ry with the CPMD package. See text for more details. ZPE stands for Zero Point Energy.

better describe exchange and correlation potentials,[35,36] and first results on vibrational spectroscopy are promising.[37,38] Rothlisberger's group has also contributed to including dispersion terms in the DFT formalism in the context of the Car−Parrinello methodology.[39,40] When dealing with charged species, as is the case here, this latter contribution is less important since the dominant interactions correspond to electrostatic forces, which are reasonably well estimated at the DFT level.

Deprotonated phosphorylated serine, noted hereafter $[pSer\text{-}H]^-$, is the first building block of a series of deprotonated phosphorylated peptides of increasing size and complexity that we characterize by combined vibrational experiments and MD simulations. DFT-based MD simulations are applied in the present theoretical investigation in order to assess the dynamics approach to the calculation of the IR spectrum of such a "model" system and its subsequent application to bigger phosphorylated peptides. Our main contribution is to quantify temperature and nonharmonic effects of $[pSer\text{-}H]^-$ in the mid-IR domain, in a direct way.

The remainder of the paper is organized as follows: part 2 is dedicated to the description of the methods used. Results are divided into three parts, with (1) the characterization of the potential energy surface of $[pSer\text{-}H]^-$ and the dynamics at room temperature, (2) the infrared spectroscopy at room temperature from Car−Parrinello dynamics, and (3) the characterization of anharmonic effects on the vibrational bands.

2. Computational Methods

2a. Static Calculations. The potential energy surface (PES) of $[pSer\text{-}H]^-$ was initially explored at the B3LYP/6-31+G(d) and BLYP/6-31+G(d) levels. The choice of this basis set follows our previous calibration work on protonated and deprotonated phosphorylated amino acids.[24−26] Harmonic frequencies have been calculated in order to check that optimized structures are minima on the PES. The structures of lowest energies, *pSer-H_1*, *pSer-H_2*, *pSer-H_3*, and *pSer-H_4* (see below) have been subsequently reoptimized at the BLYP/6-311++G(d,p) and B3LYP/6-311++G(d,p) levels, followed by harmonic frequency calculations. Moreover, the two most stable conformers (*pSer-H_1* and *pSer-H_2*) have been further optimized at the BLYP/aug-cc-pVTZ and B3LYP/aug-cc-pVTZ levels, and we also have performed single point calculations for *pSer-H_3* and *pSer-H_4* at the BLYP/aug-cc-pVTZ using the BLYP/6-31+G(d) optimized geometries. This calibration study was carried out to check that the energetic order of the low energy structures was unchanged. Energies are reported in Table 1. All calculations were performed using the Gaussian03 package.[41]

2b. DFT-Based Molecular Dynamics Simulations. The DFT-based Car−Parrinello molecular dynamics (CPMD) simulations performed in this work follow the general setup of our previous simulations.[12,14,28,31,32] All simulations were carried out with the CPMD package.[27] We used the Becke, Lee, Yang, and Parr (BLYP) gradient-corrected functional[42,43] for the exchange and correlation terms. The one electron orbitals are expanded in a plane-wave basis set with a kinetic energy cutoff of 90 Ry restricted to the Γ point of the Brillouin zone. Medium soft norm-conserving pseudopotentials of the Martins-Trouillier type[44] are used. The core−valence interaction in C, N, and O is treated by *s* and *p* potentials with pseudization radii of 1.23, 1.12, and 1.05 au, respectively (taking the same radius for *s* and *p*), while H atoms are treated as an *s* potential with a 0.5 au radius. The core−valence interaction in (neutral) P is treated by *s*, *p*, and *d* potentials with pseudization radii of 1.5 (*s*), 1.5 (*p*), and 1.09 (*d*) (in au). We have added *d*-states taken from the $1s^2 2s^2 2p^6 3s^1 3p^{1.75} 3d^{0.25}$ configuration of the ion. Energy expectation values are calculated in reciprocal space using the Kleinman-Bylander transformation.[45]

The value of 90 Ry for the energy cutoff of the plane wave expansion of the wave function has been chosen with the following scheme. We have checked that the difference of energy between the different structures identified in the all electron BLYP/6-31+G(d) geometry optimizations is correctly reproduced with single point energy calculations using the plane wave basis set and the pseudopotentials of the Car−Parrinello setup. Two energy cutoff values for the plane-wave expansion have been checked, 90 and 110 Ry. Both give the same energy order and nearly identical energy differences with respect to the most stable conformer, as reported in Table 1. As there is no difference between the two plane wave basis sets, we chose the lower energy cutoff of 90 Ry. The energy differences given by the plane-wave

Table 2. Average Ionic Temperatures (Kelvin) Obtained in the Microcanonical Car-Parrinello Molecular Dynamics Simulations Performed in This Work

CPMD	<T>	<T_C>	<T_H>	<T_O>	<T_N>	<T_P>
17.1 ps	13 ± 2	18 ± 4	12 ± 2	12 ± 1	13 ± 0	11 ± 2
17.9 ps	245 ± 30	220 ± 25	232 ± 41	267 ± 22	281 ± 36	237 ± 8
13.9 ps	298 ± 23	297 ± 1	309 ± 37	290 ± 20	292 ± 5	268 ± 30

calculation are very similar to those obtained at the all electron BLYP/aug-cc-pVTZ level. Note that the BLYP and B3LYP energy differences are nearly identical, apart for isomers *pSer-H_3* and *pSer-H_4* for which the energy difference with respect to the conformation of lowest energy (*pSer-H_1*) is underestimated by the BLYP calculations (∼1.5 kcal/mol). This has however no consequence in the present work, as it turns out that these salt bridge conformations are not explored during the dynamics.

Car−Parrinello dynamics (CPMD) were performed in the microcanonical ensemble (at constant volume and internal energy) using a fictitious electron mass of 400 au and a time step of 4 au (0.096 fs), see our previous papers for further details.[12,14,28,31,32] Gas-phase simulations were carried out with the decoupling technique of Martyna and Tuckerman[46] in order to eliminate the effect of the periodic images of the charge density. A cubic box length of 20 Å was selected after performing a series of wave function optimizations of *pSer-H_1* and *pSer-H_2* isomers in boxes of increasing length. We found that from 20 Å on, the electronic energy of the isolated molecule is converged within 10^{-5} au, which ensures that the wave function of the isolated anion is entirely contained in the box cell. CPMD simulations reported here consist of two steps: an equilibration phase of 1−2 ps partially performed with a control of temperature through velocity rescaling, followed by data collection over trajectories of ∼14−18 ps where molecular dynamics are strictly microcanonical. We have performed three dynamics, one at ∼20 K (17.1 ps) and two at ∼300 K (17.9 and 13.9 ps). Room temperature has been chosen for consistency with the average temperature of the IR-MPD experiments. Initial velocities were chosen in a Boltzmann distribution centered at the desired temperature. The average molecular temperature and average temperatures of each atomic type obtained for the simulations are shown in Table 2. Equipartition of energy over all degrees of freedom is globally respected in each simulation (keeping in mind that definition of temperature for such a small system is always questionable). It is especially difficult to achieve a proper equipartition of energy for low temperature dynamics within the short time-scale that can be afforded by CPMD. One can thus note that, on average, only the carbon atoms are slightly too warm during the low temperature dynamics; we will come back to this point when discussing infrared intensities. The final "room temperature" infrared spectrum presented here has been averaged over the two trajectories.

The calculation of the infrared absorption coefficient, $\alpha(\omega)$, makes use of the relation involving the Fourier transform of the time correlation of the total dipole moment of the molecule $\mathbf{M}(t)$, according to ref 29

$$\alpha(\omega)n(\omega) = \frac{2\pi\beta\omega^2}{3cV}\int_{-\infty}^{+\infty}\langle \mathrm{M}(t)\mathrm{M}(0)\rangle e^{i\omega t}dt \qquad (1)$$

where $\beta = 1/k_BT$, $n(\omega)$ is the refractive index, c is the speed of light in vacuum, and V is the volume of the simulation box. The angular brackets in formula (1) indicate a statistical average. Note that in this formula we have taken into account a quantum correction factor (multiplying the classical line shape) of the form $\beta\hbar\omega/(1\text{-}e^{-\beta\hbar\omega})$, which was shown to give the most accurate results for IR intensities.[31,32] For a complete discussion on quantum corrections, we refer the reader to refs 47 and 48. The IR spectrum is defined as the product $\alpha(\omega)n(\omega)$, with ω in cm^{-1}. $\mathbf{M}(t)$ is the dipole moment of the molecule at time t, which is the sum of the nuclear and electronic contributions. The dipole moment of the box cell is calculated with the Berry phase representation, as implemented in the Car−Parrinello framework and described in details previously (see for instance ref 31). The final spectra were smoothed with a window filtering applied in the time domain, which corresponds roughly to the convolution of the bare spectrum by a 10−20 cm^{-1} width Gaussian function. This convolution has the only purpose to remove the numerical noise arising from the finite length of the Fourier transform of eq 1. We have checked that the durations of the dynamics performed here are sufficient to obtain converged IR intensities (i.e., the latter are not modified upon increasing the dynamics duration).

Comparison of IR absorption intensities calculated within either the static or the dynamics formalisms to the ones obtained in IR-MPD experiments is certainly not well understood. Equation 1 for IR signal relies on linear response theory and is strictly valid for one-photon linear IR absorption spectroscopy. IR-MPD on the other hand is a multiphoton IR absorption process leading to the fragmentation of the molecule: the recorded signal is the fragmentation yield as a function of the IR excitation wavelength. It is thus an indirect measurement of IR absorption, in contrast to the usual linear IR spectroscopy. Calculations and experiments are therefore not directly comparable for band intensities, giving rise to possible discrepancies. The direct simulation of IR-MPD spectra, with a clear theoretical expression of signal intensity in terms of dynamical quantities, remains an open question.

In all of our previous applications of CPMD to IR spectroscopy (gas and liquid phase calculations in the 800−2000 cm^{-1} range)[12,14,28,31,32] we have systematically found that our calculated infrared spectra have to be blue-shifted by 100 cm^{-1} so that all of the calculated bands are aligned with their experimental counterparts. As a consequence, although our CPMD calculations do not give the proper absolute values of band positions, they do yield accurate band-gaps between the active bands. We stress again that a *global translation* is applied to the spectrum, not a scaling factor. This empirical finding is in contrast to static *ab initio* calculations where a scaling factor is used to correct the theoretical predictions with respect to the observed frequencies (in order to compensate for both the level of theory and anharmonicities). The origin of this is at the moment unclear to us. Effects of the fictitious mass, which leads to instantaneous Car−Parrinello forces being different

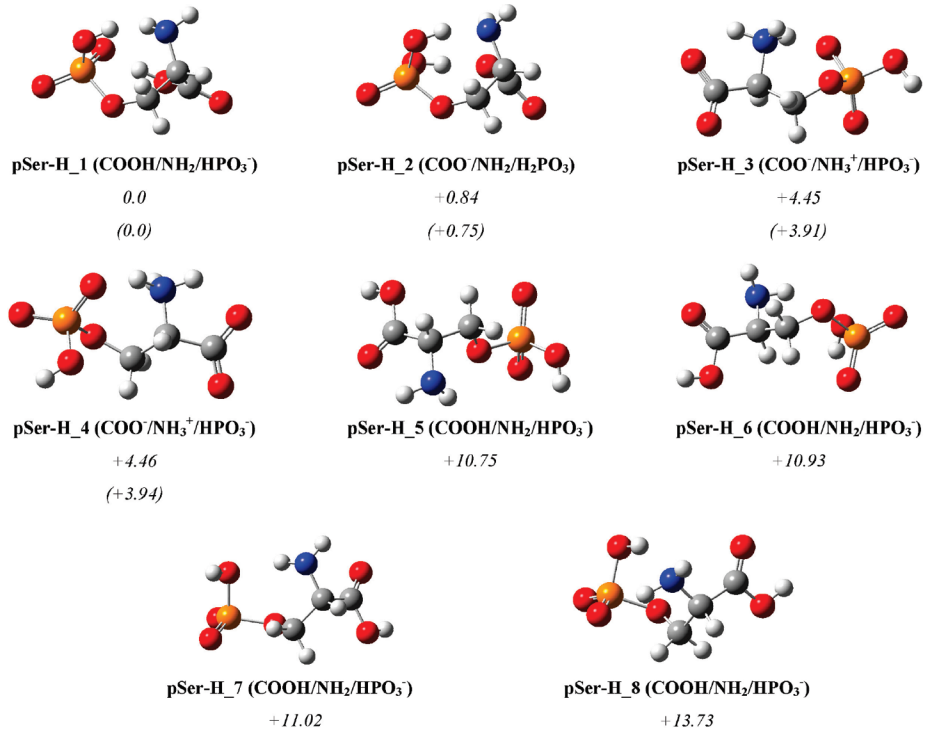

Figure 1. Schematic representation of the eight isomers of the deprotonated phosphorylated Serine $[pSer\text{-}H]^-$ identified in this work. Relative energies between the isomers have been reported using the CPMD setup (plane-wave basis set of 90 Ry and pseudopotentials) and in parentheses using the all electron BLYP/6-311++G** calculations (either optimized geometries or single point energies on the BLYP/6-31+G(d) geometry optimizations, see Table 1).

from Born−Oppenheimer (BO) ones whatever the fictitious mass value[49,50] is certainly important, and indeed the blue-shift of 100 cm^{-1} can be reduced when performing CPMD with smaller fictitious masses for the propagation of the electronic wave function. This is though at the cost of more expensive simulations. However, it has been demonstrated[49,50] that the CP forces can be brought into good agreement with the BO forces by simply rescaling the nuclear masses (thus leading to "dressed atoms"). Applying the mass scaling procedure[49] and averaging the results over all atoms of $[pSer\text{-}H]^-$, we find that blue shifts of 25 cm^{-1} and 100 cm^{-1} have to be applied, for the harmonic (20 K) and nonharmonic (300 K) dynamics performed in the present work, respectively. We have hence recovered the 100 cm^{-1} translation empirically found in our previous dynamics at 300 K. The 25 cm^{-1} translation nicely leads to the alignment of the harmonic CPMD spectrum (13 K) with the 0 K all electron spectrum computed at the BLYP/aug-cc-pVTZ level of theory (see Figure 1 in the Supporting Information and further details in part 3 below). In the rest of the paper, the above-mentioned translations have been applied to the calculated spectra. Note that performing a Born−Oppenheimer dynamics (free from the fictitious mass) remains about 10 times slower than a Car−Parrinello dynamics (within the CPMD code). This explains why vibrational spectroscopy calculations are performed with the CP algorithm despite the consequences of the use of the fictitious mass on absolute vibrational frequencies.

Assignment of the vibrational bands extracted from MD simulations has been achieved with the localization and decomposition procedure developed previously[51,52] with the associated Potential Energy Distribution (PED) quantification. This procedure goes beyond the Vibrational Density Of States (VDOS) analysis usually performed in the literature. Assignments have been done in terms of nonredundant Pulay internal coordinates (see ref 51 for more details). They are given for the two trajectories performed in this work, i.e. harmonic low-temperature dynamics and nonharmonic room-temperature dynamics. As presented in refs 51 and 52, our assignment method turns out to provide "effective normal modes". The ones extracted from the low-temperature harmonic dynamics are identical to the harmonic normal modes that are calculated by diagonalizing a Hessian matrix. The "effective normal modes" extracted from the 300 K nonharmonic dynamics take into account temperature and anharmonicities of the dynamics. We have compared the vibrational assignments for the harmonic and nonharmonic dynamics in order to assess how the modes can be modified by anharmonicities and temperature. Furthermore, we take the opportunity to quantify how much the room-temperature modes resemble or differ from the pure harmonic normal modes by projecting the room-temperature modes onto the normal modes extracted from the harmonic dynamics. In that way, we are able to assess how the harmonic normal modes can be relevant for the interpretation of the vibrational bands that are recorded at finite temperature in the experiment. Results will be presented in the following section.

3. Results

3.1. Geometry Optimizations. All electron geometry optimizations led to the eight isomers/conformers depicted in Figure 1. Their relative energies are gathered in Table 1. Three families can be identified, depending on the proton-

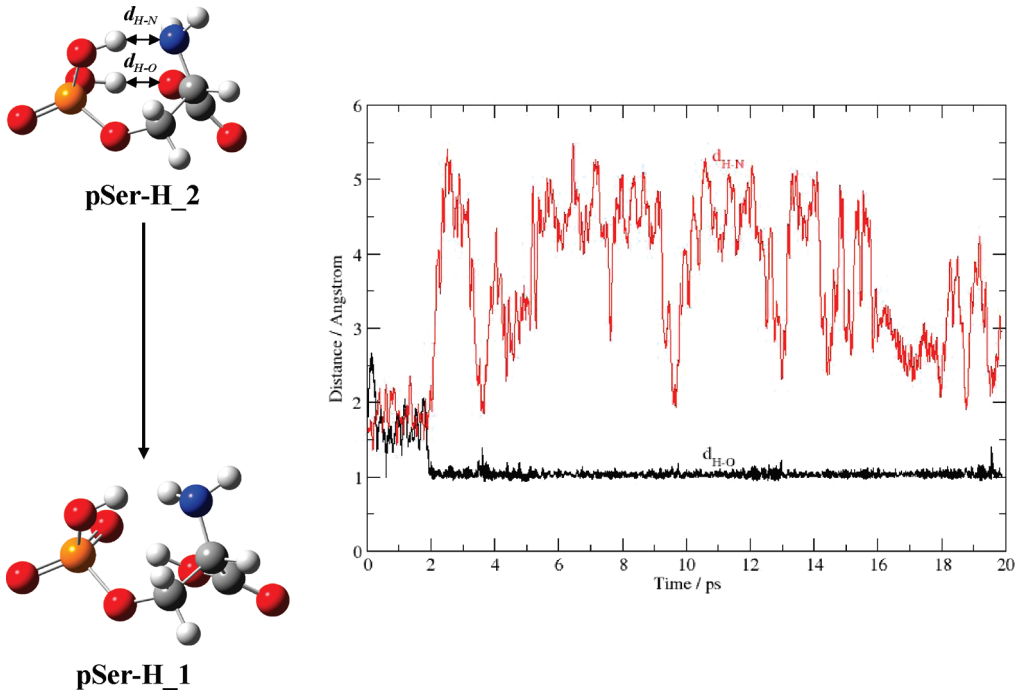

Figure 2. Car−Parrinello molecular dynamics simulation at 300 K. Evolution with time of (PO)H.. .N(H_2) and (PO)H.. .OCO distances, in order to illustrate the conformational dynamics between "pSer-H_1" and "pSer-H_2" types of geometries during the dynamics: proton transfer from POH to the acid.

ation state of the phosphate group and the N- and C-termini of the amino acid (OPO_3H_2/OPO_3H^-, NH_3^+/NH_2, COOH/COO^-). They are respectively identified as (1) deprotonated on the phosphate group (HPO_3), see structures *pSer-H_1*, *pSer-H_5*, *pSer-H_6*, *pSer-H_7*, and *pSer-H_8* in Figure 1, (2) deprotonated on the acid (COO^-), see structure *pSer-H_2*, and (3) salt-bridge structures with deprotonated phosphate and acid, and protonated amine, see *pSer-H_3* and *pSer-H_4*. Structures *pSer-H_1* and *pSer-H_2* are found to be the lowest in energy, with an energy difference smaller than ∼1.5 kcal/mol whatever the density functional and basis set employed. The energy difference is decreased to less than ∼1.0 kcal/mol when including the zero point vibrational energy, see Table 1. The BLYP and B3LYP relative energies are in excellent agreement with each other, with less than 0.5 kcal/mol difference in most cases (pSer-H_3, pSer-H_4, and pSer-H_5 have slightly larger differences of 1−1.5 kcal/mol).

pSer-H_1 and *pSer-H_2* can be seen as folded geometries displaying strong hydrogen bonds between the phosphate and amino groups. They differ by a simple proton transfer between the phosphate and the carboxylate. The conformations of higher energy mostly display less folded geometries that therefore give less opportunity for the phosphate group to form hydrogen bonds with the amine or the acid.

The geometry of *pSer-H_1* displays two strong and one weak H-bonds. The two strong H-bonds are formed between the COOH and one PO (COOH...OP H-bond distance and angle are respectively 1.529 Å and 172° at the BLYP/aug-cc-pVTZ level) and between the NH_2 and the same PO (2.009 Å and 140° at the BLYP/aug-cc-pVTZ level). A weak H-bond is formed between the amine and the POH (H_2N...HOP = 2.281 Å and 140° at the BLYP/aug-cc-pVTZ level). In the geometry of *pSer-H_2* the two POH groups are involved in strong hydrogen bonds, one with the carboxylate COO^-...HOP (1.597 Å and 178° at the BLYP/aug-cc-pVTZ level) and one with the amine H_2N...HOP (1.758 Å and 160° at the BLYP/aug-cc-pVTZ level).

3.2. Dynamics at 300 K. We have performed two dynamics at room temperature. The average temperatures obtained are reported in Table 2. One dynamics was begun from the optimized geometry *pSer-H_2*. As illustrated in Figure 2, this geometry changes within 2 ps of dynamics, when a proton transfer occurs from the POH group initially H-bonded to COO^-. This leads to an isomer bearing a deprotonated phosphate and a protonated acid. We never observed any proton transfer back from the COOH to the phosphate group during the dynamics. Figure 2 also shows that the remaining POH group is highly fluxional, with very little probability for a POH...NH_2 hydrogen bond. Note that the proton transfer occurs during the period of thermalization process of the dynamics, but we have checked that this event is not related to the velocity rescaling procedure, as the latter only takes place during the first 500 fs of thermalization, well before the proton transfer event. In order to shed some light as to why no proton transfer back to the phosphate group is observed during the length of our dynamics, we have extracted the free energy profile of the proton transfer from the dynamics. This is calculated as -kT lnP(H) where P(H) is the probability histogram related to the sampling of the reaction coordinate for the proton transfer between the phosphate and the acid along the dynamics. We found that the free energy barrier from pSer-H_2 to the transition state is ∼0.8 kcal/mol and that the free energy barrier from pSer-H_1 to the transition state is ∼3.1 kcal/mol. These values explain why the energy barrier is easily overcome during a room temperature dynamics taking place in the basin of pSer-H_2 but is not so easily overcome once trapped in the basin

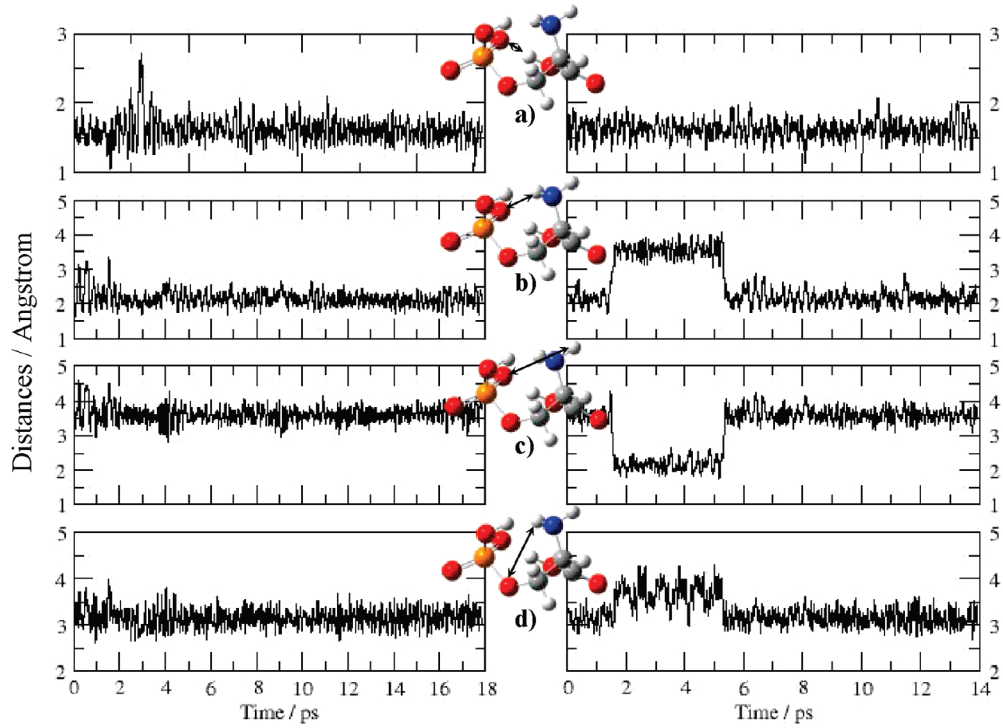

Figure 3. Car−Parrinello molecular dynamics simulations at 300 K. Evolution with time of selected possible hydrogen bond distances reported for the two room temperature dynamics performed in this work (average temperatures of the dynamics - see Table 2: 245 K (left) and 298 K (right)). Selected distances are illustrated with arrows.

of pSer-H_1. Note that the addition of nuclear quantum effects is expected to decrease these values. On the other hand, the free energies calculated from the optimized geometries of *pSer-H_1*, *pSer-H_2* and the saddle-point connecting them, within the harmonic approximation, give a slightly different view. Depending on the basis set used, the free energy barrier to be overcome from pSer-H_2 varies in the range 0.2/−0.2 kcal/mol and the one to be overcome from pSer-H_1 is 0.3/0.7 kcal/mol. These values suffer from the harmonic approximation though, which is not the case for the free energies extracted from the dynamics. Yet short propagation times may lead to an overestimation of the barriers. Low energy barriers would lead to the dynamical sampling of regions of the PES mostly outside the minima, while higher energy barriers would do the opposite. The latter is confirmed by the present dynamics and thence very good reproduction of the IR-MPD signatures, *vide infra*, therefore supporting the free energy values extracted from the dynamics.

The last configuration (positions and velocities) of this dynamics was used as a starting point for the second dynamics performed here, with an initial rescaling of velocities and thermalization procedure in order to randomize the velocities.

The two dynamics were propagated in the microcanonical ensemble for 17.9 and 13.9 ps, respectively, and we find that they both take place within the basin of "pSer-H_1", with small distortions of the skeleton from the optimized geometry: the skeleton dihedrals differ by no more than 20° from those of the optimized configuration. As reported in Table 2, the average temperatures of the dynamics are 245 and 298 K.

As reported in Figures 3 and 4, we can see that a PO...HOC=O H-bond is present at room temperature at a very short distance of ∼1.61 Å on average and is almost never broken (Figure 3a). PO is, on average, simultaneously involved in a supplementary weak H-bond with one of the hydrogen atoms of the amine. The average PO...HNH distance is ∼2.16 Å, and we can observe an exchange of the amine hydrogen involved in the H-bond over time (Figure 3b-c). There is thus enough internal energy at room temperature to overcome the barrier to the rotation of the amine group and the associated breaking/reforming of the H-bond with the neighboring PO group. Note that Figure 3d indeed confirms the rotation of the NH_2 group. There is no POH...NH_2 H-bond formed, on average (Figure 4a). This distance indeed evolves between 2.0 and 5.5 Å along the two dynamics, displaying transient very short periods of time during which a H-bond can actually be seen. At room temperature, there is an easy rotation around the P−OH bond, as nicely illustrated by the time evolution of the two POH...OP distances (Figure 4b-c): the H atom is seen to alternate short intermolecular distances with the two PO oxygens along the time. This rotation explains why no POH...NH_2 H-bond can be formed during the dynamics. On average, the phosphate group is therefore composed of one free PO bond, while the second PO is involved in two simultaneous hydrogen bonds with the amine N−H (weak H-bond) and the acid O−H (strong H-bond). POH is free of any hydrogen bonding, on average.

3.3. Infrared Spectroscopy at 300 K. The infrared spectrum extracted from the room temperature dynamics is shown in Figure 5, together with the experimental IR-MPD spectrum. We find that the calculated spectrum of $[pSer-H]^-$ at 300 K displays a good agreement of band widths with the IR-MPD experiment. The positions of the bands obtained in the present calculation differ by 10−20 cm^{-1} from their

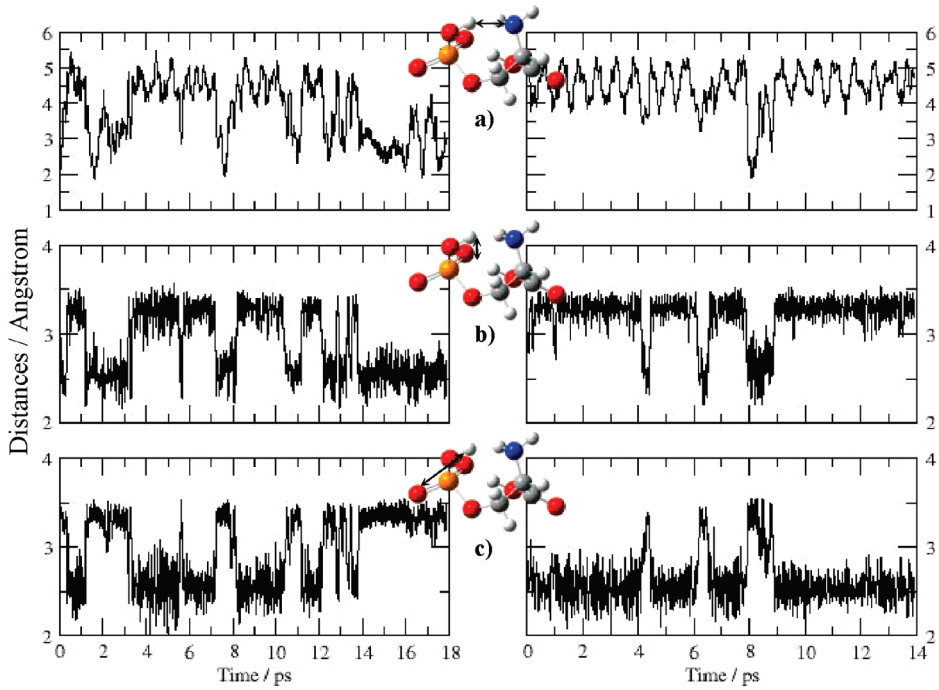

Figure 4. Car−Parrinello molecular dynamics simulations at 300 K. Evolution with time of selected possible hydrogen bond distances reported for the two room temperature dynamics performed in this work (average temperatures of the dynamics - see Table 2: 245 K (left) and 298 K (right)). Selected distances are illustrated with arrows.

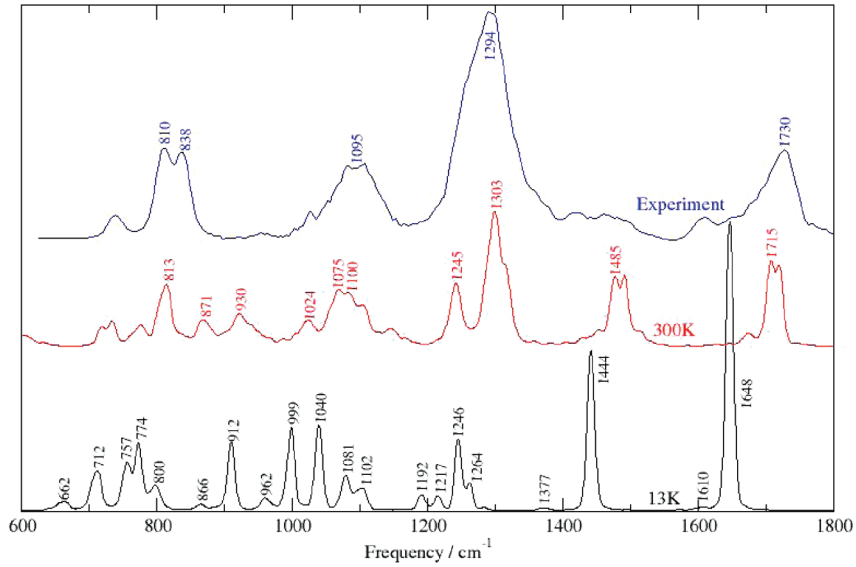

Figure 5. Infrared spectrum of $[pSer-H]^-$ extracted from the harmonic Car−Parrinello dynamics (13 K on average, bottom of the figure) and the room temperature nonharmonic Car−Parrinello dynamics (271 K as the average from the two CPMD performed in the present work, medium of the figure). The experimental IRMPD spectrum is reported at the top of the figure. Wavenumbers displayed on top of the bands are reported in cm^{-1}. Assignment of the bands can be found in the text. See Table 3 for the summary of the vibrational interpretation of the IRMPD spectrum as found from the room temperature dynamics performed in the present work.

IR-MPD values, while the experimental band gaps are very well reproduced by our calculation.

The following assignments of the vibrational bands are summarized in Table 3. The two bands located in the 1600−1800 cm^{-1} region of the spectrum are respectively assigned to the C═O stretching (∼1715 cm^{-1}) and to the N−H scissoring (∼1675 cm^{-1}) motions. The shape and breadth of the experimental feature at 1660−1740 cm^{-1} suggests that it is composed of two bands, as indeed our calculations show. Its higher frequency part is consistent with a carboxylic group as opposed to a carboxylate.[26,53] Note that the low intensity experimental band at ∼1600 cm^{-1} has no counterpart in our calculation.

The bands in the 1500−700 cm^{-1} calculated spectrum are related to vibrations predominantly arising from the phosphate and to a lesser extent from the acid. The band located between 1520 and 1420 cm^{-1} with a sharp feature at 1500−1470 cm^{-1} is due to C−OH stretching and bending,

Table 3. Summary of the Vibrational Interpretation of the IRMPD Spectrum As Found from the Room Temperature Dynamics Performed in the Present Work[a]

IRMPD band position (cm^{-1})	assignments from 300 K CPMD
1730	C═O stretch (acid)
1294	free PO stretch (phosphate)
1095	H-bonded PO stretch (phosphate)
810−838	P−OH stretch (phosphate)

[a] The interpretation reported here corresponds to the main assignments from the dynamics. See Text-Part 3, for the details.

while the ∼1430 cm^{-1} shoulder is due to the adjacent CH_2 rocking motion. The higher frequency part of the ∼1320−1220 cm^{-1} band arises from the free PO stretching (∼1303 cm^{-1}), also with a very low participation of the H-bonded PO stretching, and the lower frequency part is due to the stretching-bending of the C−OH (∼1245 cm^{-1}). The COH motions are thus split into two bands separated by ∼240 cm^{-1}. Within the large feature between 1000 and 1120 cm^{-1}, the main peak at ∼1075 cm^{-1} comes from the stretching motion of the hydrogen bonded PO. The two shoulders on both sides of this broadband are related to N−C stretching and NH_2 wagging around the C−N bond (also noted C-NH_2 wagging) (∼1145 cm^{-1}) and to combined skeleton OCC scissoring and C-NH_2 wagging (∼1024 cm^{-1}). Globally, the 1000−700 cm^{-1} calculated domain appears to suffer the largest band displacements with respect to experiment. The low intensity band calculated at ∼930 cm^{-1}, due to a combination of N−C stretching and POC bending, has no experimental counterpart. The ∼871 cm^{-1} band arises from the skeleton OCC scissoring motion, while stretching of the P−OH gives rise to the main ∼813 cm^{-1} peak. The 700−775 cm^{-1} bands come from more delocalized skeleton torsions. At least 2 peaks can be seen in the 800 cm^{-1} IR-MPD band. It is conceivable that the 813 cm^{-1} peak is well reproduced by our calculation, while the 871 cm^{-1} calculated band is blue-shifted by 32 cm^{-1} relative to experiment.

The IRMPD experimental active bands in the 1400−1800 cm^{-1} domain are therefore signatures of the acid and amine groups of the amino acid. In fact, the signatures of the acid (C═O at higher frequencies and COH at lower frequencies) are mainly observed, while the signature of the amine can only be seen in the tail of the C═O band. The three remaining experimental bands in the intermediate 800−1400 cm^{-1} range come solely from the phosphate group. There is a band gap of 228 cm^{-1} between the signatures of the free (1303 cm^{-1}) and H-bonded (1075 cm^{-1}) PO groups, while the band at lower frequency reflects the vibrations of the phosphate POH group. The signature of the H-bonded PO is red-shifted from the free PO, as expected upon formation of a hydrogen bond, and the large 228 cm^{-1} red-shift obtained here reflects the energetically strong H-bond that is formed between PO and COH.

All of these bands reproduce the IR-MPD bands in both positions and shapes. The present dynamical treatment thus appears to capture adequately the anharmonicities and mode couplings in such a way that most band positions and shapes are rather accurately reproduced.

3.4. Harmonic Spectra. In order to obtain a more detailed understanding of the vibrational signatures of $[pSer-H]^-$ at room temperature, it is useful to compare them to those of the harmonic spectrum. The latter has been calculated in two different ways: low temperature CPMD and static calculations (all-electron Gaussian calculations[41] and Hessian-based calculation through the CPMD package). At very low temperatures (an average temperature of 13 ± 2 K was used here, see Table 2) the dynamics becomes effectively harmonic to a very good approximation. If the exact same procedure were used to calculate the energy, this calculation would be nearly identical to the more common Hessian-based calculation at the optimized geometry, as shown in Table 3 of the Supporting Information. Note that in principle, even at the low temperature used here for the dynamics, very small barriers on the potential energy surface (e.g., 10 cm^{-1}) could be overcome, leading to deviations from the harmonic approximation. In order to evaluate whether this occurs in the present case, root-mean-square deviations on bond-lengths and bond-angles along the 13 K dynamics are presented: bond-lengths fluctuate in the range 0.004−0.009 Å (apart H-bond distances that fluctuate by up to 0.02−0.03 Å) and bond-angles vary within 1.9−3.0°. These very small variations of the molecular geometry confirm that the harmonic approximation of the potential energy surface is correct in the 13 K dynamics. Such small fluctuations cannot therefore have any significant influence on the calculated frequencies.

Although the same density functional is used (BLYP), the CPMD calculations (dynamics and Hessian-based) involve a plane wave valence basis set together with core pseudopotentials, instead of the all-electron Gaussian basis set used in the Hessian-based static calculation. Thus the low temperature CMPD dynamics calculation has a 2-fold goal: (1) calculate the harmonic CPMD IR spectrum and compare it to the static calculations in order to validate our CPMD setup and (2) discuss vibrational anharmonicities of $[pSer-H]^-$ at room temperature by comparing the low and room temperature spectra extracted at exactly the same level of theory. Furthermore, comparison of the CPMD Hessian-based harmonic spectrum to the 13 K CPMD dynamics harmonic spectrum is presented in order to demonstrate that the average 25 cm^{-1} translation that we apply to the 13 K dynamics harmonic spectrum (due to the use of the fictitious mass in the dynamics) is correct.

The static harmonic normal-mode frequencies of the conformation of lowest energy (*pSer-H_1*) calculated with the BLYP and B3LYP functionals and three different basis sets are reported in Table 1 in the Supporting Information (no scaling factor applied). For each functional investigated here, the frequencies vary on average by ±10 cm^{-1} when changing the basis set, and slight variations in some peak intensities can also be observed. The corresponding IR spectra are plotted in Figure 2 of the Supporting Information for the specific case of the aug-cc-pVTZ basis set. In this figure scaling factors of 0.9669 and 0.9962 have been applied to the B3LYP and BLYP frequencies, respectively.[54] These

values are taken from 6-311G(d,p) basis set calculations, as this is the largest basis set investigated in ref 54. BLYP and B3LYP spectra display exactly the same vibrational features, with the B3LYP frequencies being on average 10−20 cm^{-1} higher than the BLYP frequencies. The two functionals therefore perform similarly.

We performed a 17.1 ps CPMD dynamics at 13 K starting from *pSer-H_1*. As expected at such a low temperature, the average geometry obtained during the dynamics remains very close to the optimized one, as shown in Table 2 in the Supporting Information where structural parameters are reported. In particular, the three hydrogen bonds in the optimized geometry discussed above are maintained at 13 K. The only significant difference comes from the POH...N H-bond distance that is found to be 0.13 Å longer in the dynamics. This is mainly a basis set rather than a temperature effect, as this distance is optimized at 2.28 Å with the largest aug-cc-pVTZ basis set and increases with the basis set growth, to be compared to its average value of 2.33 Å from the dynamics.

The frequencies extracted from the 13 K dynamics harmonic spectrum are compared to the frequencies obtained from the Hessian-based calculation in Table 3 of the Supporting Information, all obtained within the CPMD setup. Two schemes have been applied for the Hessian-based calculation, Linear Response (LR) and Finite Difference (FD), that give identical results within 0−2 cm^{-1}. The frequencies extracted from the 13 K harmonic spectrum differ from the Hessian-based frequencies by an average 7 cm^{-1}. This is the result of the mean 25 cm^{-1} translation we apply to the dynamical spectrum to take care of the fictitious mass and not from deviations from harmonicities in the 13 K dynamics as already demonstrated above. It is worth noting that the frequencies of the movements implying heavy atoms are identically found in the spectra extracted from the dynamics and the static Hessian-based. In the rest of the paper we only make use of the harmonic spectrum extracted from the 13 K CPMD dynamics.

The harmonic CPMD IR spectrum is presented in Figure 5 together with the 300 K CPMD and the experimental IRMPD spectra. It is also shown in Figure 1 of the Supporting Information along with the all electron BLYP/aug-cc-pVTZ IR spectrum. Frequencies in the 600−1800 cm^{-1} region obtained with the 6-31+G(d), 6-311++G(d,p), and aug-cc-pVTZ basis sets using B3LYP and BLYP functionals are reported in Table 1 of the Supporting Information, for the sake of comparison. We immediately observe that the spectrum extracted from the dynamics displays the same features as the all electron BLYP spectrum, apart from slight shifts in the band positions. On average, CPMD frequencies differ by 10−20 cm^{-1} from the all electron frequencies, the largest discrepancies being observed below 800 cm^{-1}. Differences observed in the intensities can be traced back to the equipartition of energy, which is difficult to achieve at low temperature and within such a short dynamics time scale. As a consequence, the participation of cold atoms involved in active bands is underestimated (thus usually underestimating the corresponding IR intensities), while the participation of warm atoms involved in active bands is overestimated (thus usually overestimating IR intensities). As seen in Table 2, carbon atoms are, on average, the warmest atoms, which will be one main reason for the high intensities of the δ(COH) (1444 cm^{-1}) and ν(C═O) bands (1648 cm^{-1}) as well as for the 912 and 999 cm^{-1} bands whose signatures can be traced back to carbon atoms.

As for the 300 K spectrum, the 13 K harmonic spectrum in Figure 5 may be interpreted using our localization and decomposition procedure.[51,52] The bands in the 1800−1400 cm^{-1} domain are due to the stretching motion of C═O (1648 cm^{-1}) and combined stretch−bend of COH (1444 cm^{-1}). The shoulder at 1610 cm^{-1} arises from the amine scissoring motion. The main signature of the ∼1200−1300 cm^{-1} band is due to the free PO stretching (1246 cm^{-1}). The satellite bands are respectively arising from CH rocking and C−OH stretch (1264 cm^{-1}), NH_2 rocking (1217 cm^{-1}), and C−OH stretching (1192 cm^{-1}). The large 1100−800 cm^{-1} band is composed of POH bending and free PO stretch (1102 cm^{-1}), C−OH wagging (1081 cm^{-1}), CH_2 rocking (1040 cm^{-1}), H-bonded PO stretch (999 and 962 cm^{-1}), C-NH_2 wagging (912 cm^{-1}), N−C stretch (866 cm^{-1}), and COOH wagging around the C−C bond (800 cm^{-1}). The 757−774 cm^{-1} bands are assigned to the OH stretch of POH and the lower frequencies to more delocalized modes (NH_2/COOH part at 712 cm^{-1} and phosphate part at 662 cm^{-1}).

It is worth noting that the harmonic COH bending mode observed here at 1444 cm^{-1} is blue-shifted by about 200 cm^{-1} from the same bending motion of the COH group when it is not involved in hydrogen bonding as is the case for conformers pSer-H_5 to pSer-H_8, see Figure 1. Blue shifts on bending motions are expected from the formation of hydrogen bonds, and such a strong displacement reflects the energetically strong H-bond that is formed between the PO and the acid group of $[pSer\text{-}H]^-$.

3.5. Vibrational Anharmonicities and Mode Couplings at 300 K. Comparison of the spectra extracted from the harmonic (low temperature) and nonharmonic (room temperature) dynamics allows us to quantify vibrational shifts due to the combination of temperature driven conformational dynamics, vibrational anharmonicities (anharmonic oscillators and mode couplings), and dipole anharmonicities (beyond the electrical harmonic approximation), since band shifts are the result of these combined effects. The anharmonic spectrum is globally shifted toward higher frequencies with respect to the harmonic spectrum, with an average blue-shift of ∼50−60 cm^{-1}. Though blue-shifts upon anharmonicities and mode couplings have already been observed by Gerber et al. on other peptide models in the same frequency range,[55−58] the systematic blue-shift obtained here is puzzling, and might be entirely fortuitous and due to the DFT PES. However, it remains that upon this blue-shift the anharmonic spectrum is perfectly aligned with the IR-MPD spectrum and provides a very good account of the experimental signatures.

Following ref 55, we define the percentage of anharmonicity of a mode by $(\nu_{anharm} - \nu_{harm})*100/\nu_{anharm}$ where ν_{harm} and ν_{anharm} are respectively the harmonic and anharmonic frequencies of a given mode. In the frequency region investigated here, we find that this percentage is 4% on

average, apart for the stretching movements of the H-bonded PO (1075 cm^{-1} in the 300 K anharmonic spectrum) and free P−OH (813 cm^{-1} in the 300 K anharmonic spectrum), where the anharmonicities are respectively 10.5% and 7%. Interestingly, the C−OH stretching movement (1245 cm^{-1} in the 300 K anharmonic spectrum) is only 4% anharmonic, even though this group is hydrogen bonded to PO.

As described in the method section above, we are able to describe and quantify the anharmonic vibrational modes in terms of the harmonic modes. We find that the C═O stretching, NH_2 scissoring, and COH bending modes in the 1400−1800 cm^{-1} domain can be fully described by the corresponding harmonic modes, implying that these modes undergo no anharmonic coupling to other modes. As a consequence, the blue-shifts of these bands at 300 K relative to 13 K and the average 4% anharmonicity of these modes appear to be due to the intrinsic anharmonicities arising from the potential energy surface and transition dipole moment of the related vibrational motions.

On the contrary, the three phosphate bands located at 1303, 1075, and 813 cm^{-1} display couplings to several harmonic modes. Hence, the 1303 cm^{-1} free PO stretch anharmonic mode has two major components, 60% from the 1246 cm^{-1} PO stretch harmonic normal mode and 25% from the POH bending harmonic normal mode at 1102 cm^{-1}. The 1075 cm^{-1} H-bonded PO stretch is a stiffer vibrational mode as it displays less mode coupling, though two major components are found: 76% of this mode is represented by the 999 cm^{-1} PO stretch harmonic normal mode, together with 7% of the C−OH wagging 1081 cm^{-1} harmonic mode. The 813 cm^{-1} mode displays an intermediate state in mode couplings, with 69% and 18% from the 774 and 757 cm^{-1} harmonic modes, respectively, although both harmonic modes correspond to a splitting of the harmonic P−OH stretch. These couplings certainly participate to the blue shifts of the bands obtained at room temperature.

4. Conclusions

The IR spectrum of deprotonated phosphorylated serine $[pSer-H]^-$ extracted from the present DFT-based room temperature molecular dynamics simulations gives a good account of the experimental IRMPD spectrum. Band positions and shapes are in very good agreement with the experiment, and, as already mentioned, intensities obtained from the one-photon absorption calculations performed here should not be directly compared to the fragmentation yield recorded in the experiment. The comparison of the room temperature calculated spectrum to the low temperature harmonic one calculated at the same level allows for detailed insight into temperature effects. It is found that temperature induces large changes in the IR spectrum, as illustrated by the blue shifts of a number of the main bands observed from 13 to 300 K. These shifts, the subsequent merging of certain bands and changes in their assignments, the broadening of the bands, are direct results of anharmonicities (from both the potential energy surface and the dipole moment) and mode couplings that are naturally included in the room temperature dynamics.

It is clear that vibrational anharmonic effects probed in molecular dynamics depend on the temperature of the simulation, as recently shown in ref 59. The present investigation shows that room-temperature dynamics of $[pSer-H]^-$ (expected temperature of the reference IR-MPD experiment) provides a theoretical spectrum that convincingly agrees with the experiment. The same agreement cannot be achieved with harmonic calculations, implying that anharmonicities and mode-couplings are appropriately probed in our room-temperature simulations.

The room temperature dynamics of $[pSer-H]^-$ shows a rather geometrically stiff molecule, with small distortions of the skeleton observed from the optimized geometry. Only the POH and NH_2 groups appear to be significantly fluxional. The vibrational bands recorded in the mid-IR 1800−700 cm^{-1} region predominantly arise from the deprotonated phosphate and to a lesser extent from the acid. No significant participation from the amine is observed in this region, although it is contained in the 1730 cm^{-1} IR-MPD broadband. A large blue-shift and a rather spectacular change of band shape is observed for the C═O stretching band at 1720 cm^{-1}. The bump observed in the 1400−1500 cm^{-1} region in the IRMPD spectrum is a direct probe of the protonation of the acid, as it is due to the COH bending. The three main bands in the 1400−800 cm^{-1} experimental spectrum are the signatures of the deprotonated phosphate with two bands demonstrating that there is a free PO (1294 cm^{-1} in the IR-MPD) and a strongly hydrogen bonded PO (1095 cm^{-1} in the IR-MPD). The low frequency P−OH stretching (around 830 cm^{-1} in the IR-MPD) reflects the fluxional rotating POH group, not involved in hydrogen bonding.

The analyses of the harmonic and nonharmonic modes performed here have shown that the percentage of anharmonicity in the vibrational modes is 4% on average, but that they are larger for the stretching movements of the H-bonded PO and free P−OH, where the anharmonicities are respectively 10.5% and 7%. Moreover, the assignment of the high frequency 1800−1400 cm^{-1} bands arising from the protonated acid has been shown to be identical to the harmonic modes. This is not true anymore in the 1400−700 cm^{-1} region, where the nonharmonic assignments show mode couplings arising from two predominant harmonic modes. These couplings are expected to participate to the blue-shifts of the bands that allow for a good agreement with the IR-MPD experiment.

The importance of taking temperature effects into account has been demonstrated here for the model phosphorylated serine amino acid. It is expected that the relevance of these effects will be even larger for peptides of increasing size and complexity. Going further down to lower frequency regions of the vibrational spectrum is also likely to strengthen mode couplings and anharmonicities. Calculation of IR spectra through molecular dynamics simulations will enable the proper modeling of these features. This is where our combined experiments and calculations are currently heading.

Acknowledgment. The authors thank ANR-Probio for financial support (PostDoc position of A.C) and IDRIS (Orsay, France) for a generous allowance of computer time. This work was performed using HPC resources from GENCI-IDRIS

(Grant 2009-i2009082073). The IRMPD spectrum was recorded at the infrared laser center CLIO in Orsay, France. This was made possible by the support of the European Union through the EPITOPES project (NEST 15637).

Supporting Information Available: Car−Parrinello molecular dynamics and all electron geometry optimizations performed. This material is available free of charge via the Internet at http://pubs.acs.org.

References

(1) Cohen, P. *Trends Biochem. Sci.* **2000**, *25*, 596–601.

(2) Sefton, B. M.; Hunter, T. In *Protein phosphorylation*; Academic Press: 1998.

(3) Johnson, L. N.; Lewis, R. J. *Chem. Rev.* **2001**, *101*, 2209–2242.

(4) Espinoza-Fonseca, L. M.; Kast, D. T. D. D. *J. Am. Chem. Soc.* **2008**, *130*, 12208–12209.

(5) Mandell, D. J.; Chorny, I.; Groban, E. S.; Wong, S. E.; Levine, E.; Rapp, C. S.; Jacobson, M. P. *J. Am. Chem. Soc.* **2007**, *129*, 820–827.

(6) Nakamoto, K. *Infrared and Raman Spectra of Inorganic and Coordination Compounds. Parts A and B*; New York, 1997.

(7) Lemaire, J.; Boissel, P.; Heninger, M.; Mauclaire, G.; Bellec, G.; Metsdagh, H.; Simon, A.; Caer, S. L.; Ortega, J. M.; Glotin, F.; Maître, P. *Phys. Rev. Lett.* **2002**, *89*, 273002.

(8) Maître, P.; Caer, S. L.; Simon, A.; Jones, W. D.; Lemaire, J.; Metsdagh, H.; Heninger, M.; Mauclaire, G.; Moissel, P.; Prazeres, R.; Glotin, F.; Ortega, J. M. *Nucl. Instrum. Methods Phys. Res. A* **2003**, *507*, 541–546.

(9) Oomens, J.; Roij, A. J. A. V.; Meijer, G.; Helden, G. V. *Astrophys. J.* **2000**, *542*, 404–410.

(10) Oomens, J.; Sartakov, B. G.; Meijer, G.; Helden, G. V. *Int. J. Mass Spectrom.* **2006**, *254*, 1–19.

(11) Balaj, O. P.; Kapota, C.; Lemaire, J.; Ohanessian, G. *Int. J. Mass Spectrom.* **2008**, *269*, 196–209.

(12) Gregoire, G.; Gaigeot, M. P.; Marinica, D. C.; Lemaire, J.; Schermann, J. P.; Desfrançois, C. *Phys. Chem. Chem. Phys.* **2007**, *9*, 3082–3097.

(13) Lucas, B.; Gregoire, G.; Lemaire, J.; Maître, P.; Glotin, F.; Schermann, J. P.; Desfraçois, C. *Int. J. Mass Spectrom.* **2005**, *243*, 105–113.

(14) Marinica, D. C.; Gregoire, G.; Desfrançois, C.; Schermann, J. P.; Borgis, D.; Gaigeot, M. P. *J. Phys. Chem. A* **2006**, *110*, 8802–8810.

(15) Oomens, J.; Polfer, N. C.; Moore, D. T.; Meer, L. v. d.; Marshall, A. G.; Eyler, J. R.; Helden, G. v. *Phys. Chem. Chem. Phys.* **2005**, *7*, 1345–1348.

(16) Polfer, N. C.; Oomens, J.; Dunbar, R. C. *ChemPhysChem* **2008**, *9*, 579–589.

(17) Polfer, N. C.; Oomens, J.; Suhai, S.; Paizs, B. *J. Am. Chem. Soc.* **2007**, *129*, 5887–5897.

(18) Polfer, N. C.; Paizs, B.; Snoek, L. C.; Compagnon, I.; Suhai, S.; Helden, G. v.; Oomens, J. *J. Am. Chem. Soc.* **2005**, *127*, 8571.

(19) Prell, J. S.; Demireva, M.; Oomens, J.; Williams, E. R. *J. Am. Chem. Soc.* **2009**, *131*, 1232.

(20) Vaden, T. D.; Boer, T. S. J. A. d.; Simons, J. P.; Snoek, L. C. *Phys. Chem. Chem. Phys.* **2008**, *10*, 1443–1447.

(21) Vaden, T. D.; Boer, T. S. J. d.; Simons, J. P.; Snoek, L. C.; Suhai, S.; Paizs, B. *J. Phys. Chem. A* **2008**, *112*, 4608–4616.

(22) Vaden, T. D.; Gowers, S. A. N.; Boer, T. S. J. A. d.; Steill, J. D.; Oomens, J.; Snoek, L. C. *J. Am. Chem. Soc.* **2008**, *130*, 14640–14650.

(23) Wu, R. H.; McMahon, T. B. *J. Am. Chem. Soc.* **2007**, *129*, 11312–11313.

(24) Correia, C. F.; Balaj, O. P.; Scuderi, D.; Maître, P.; Ohanessian, G. *J. Am. Chem. Soc.* **2008**, *130*, 3359–3370.

(25) Correia, C. F.; Clavaguera, C.; Erlekam, U.; Scuderi, D.; Ohanessian, G. *ChemPhysChem* **2008**, *9*, 2564.

(26) Scuderi, D.; Correia, C. F.; Balaj, O. P.; Ohanessian, G.; Lemaire, J.; Maître, P. *ChemPhysChem* **2009**, *10*, 1630–41.

(27) CPMD, copyright International Business Machines Corporation (1990−2008) and Max Planck Institute fuer Festkoerperforschung Stuttgart (1995−2001).

(28) Gaigeot, M. P. *J. Phys. Chem. A* **2008**, *112*, 13507.

(29) McQuarrie, D. A., *Statistical Mechanics*; Harper-Collins Publishers: New York, 1976.

(30) Cimas, A.; Vaden, T. D.; Boer, T. S. J. A. d.; Snoek, L. C.; Gaigeot, M. P. *J. Chem. Theor. Comput.* **2009**, *5*, 1068–1078.

(31) Gaigeot, M. P.; Sprik, M. *J. Phys. Chem. B* **2003**, *107*, 10344.

(32) Gaigeot, M. P.; Vuilleumier, R.; Sprik, M.; Borgis, D. *J. Chem. Theory Comput.* **2005**, *1*, 772.

(33) Todorova, T.; Seitsonen, A. P.; Hutter, J.; Kuo, I.-F. W.; Mundy, C. J. *J. Phys. Chem. B* **2006**, *110*, 3685.

(34) Guidon, M.; Schiffmann, F.; Hutter, J.; VandeVondele, J. *J. Chem. Phys.* **2008**, *128*, 214104.

(35) Zhao, Y.; Schultz, N. E.; Truhlar, D. G. *J. Chem. Theory Comput.* **2006**, *2*, 364–382.

(36) Zhao, Y.; Truhlar, D. G. *J. Chem. Phys.* **2006**, *125*, 194101.

(37) Jimenez-Hoyos, C. A.; Janesko, B. G.; Scuseria, G. E. *Phys. Chem. Chem. Phys.* **2008**, *10*, 6621–6629.

(38) Zhao, Y.; Truhlar, D. G. *Theor. Chem. Acc.* **2008**, *120*, 215–241.

(39) Lin, I. C.; Seitsonen, A. P.; Coutinho-Neto, M. D.; Tavernelli, I.; Rothlisberger, U. *J. Phys. Chem. B* **2009**, *113*, 1127–1131.

(40) von Lilienfeld, O. A.; Tavernelli, I.; Rothlisberger, U.; Sebastiani, D. *Phys. Rev. B* **2005**, *71*, 19.

(41) Frisch, M. J.; Trucks, G. W.; Schlegel, H. B.; Scuseria, G. E.; Robb, M. A.; Cheeseman, J. R.; Zakrzewski, V. G.; Montgomery, J. A., Jr.; Stratmann, R. E.; Burant, J. C.; Dapprich, S.; Millam, J. M.; Daniels, A. D.; Kudin, K. N.; Strain, M. C.; Farkas, O.; Tomasi, J.; Barone, V.; Cossi, M.; Cammi, R.; Mennucci, B.; Pomelli, C.; Adamo, C.; Clifford, S.; Ochterski, J.; Petersson, G. A.; Ayala, P. Y.; Cui, Q.; Morokuma, K.; Malick, D. K.; Rabuck, A. D.; Raghavachari, K.; Foresman, J. B.; Cioslowski, J.; Ortiz, J. V.; Stefanov, B. B.; Liu, G.; Liashenko, A.; Piskorz, P.; Komaromi, I.; Gomperts, R.; Martin, R. L.; Fox, D. J.; Keith, T.; Al-Laham, M. A.; Peng, C. Y.; Nanayakkara, A.; Gonzalez, C.; Challacombe, M.; Gill, P. M. W.; Johnson, B.; Chen, W.; Wong, M. W.; Andres, J. L.; Head-Gordon, M.; Replogle, E. S.; Pople, J. A. *Gaussian03*; Gaussian: Pittsburgh, 2003.

(42) Becke, A. *Phys. Rev. A* **1988**, *38*, 3098.

(43) Lee, C.; Yang, W.; Parr, R. G. *Phys. Rev. B* **1988**, *37*, 785.

(44) Trouillier, N.; Martins, J. L. *Phys. Rev. B* **1991**, *43*, 1993.

(45) Kleinman, L.; Bylander, D. M. *Phys. Rev. Lett.* **1982**, *48*, 1425.

(46) Martyna, G. J.; Tuckerman, M. E. *J. Chem. Phys.* **1999**, *110*, 2810.

(47) Borysow, J.; Moraldi, M.; Frommhold, L. *Mol. Phys.* **1985**, *56*, 913.

(48) Ramirez, R.; Lopez-Ciudad, T.; Kumar, P.; Marx, D. *J. Chem. Phys.* **2004**, *121*, 3973.

(49) Tangney, P. *J. Chem. Phys.* **2006**, *124*, 044111.

(50) Tangney, P.; Scandolo, S. *J. Chem. Phys.* **2002**, *116*, 14.

(51) Gaigeot, M. P.; Martinez, M.; Vuilleumier, R. *Mol. Phys.* **2007**, *105*, 2857.

(52) Martinez, M.; Gaigeot, M. P.; Borgis, D.; Vuilleumier, R. *J. Chem. Phys.* **2006**, *125*, 144106.

(53) Oomens, J.; Steill, J. D. *J. Phys. Chem. A* **2008**, *112*, 3281–3283.

(54) Irikura, K. K.; Johnson, R. D.; Kacker, R. N. *J. Phys. Chem. A* **2005**, *109* (37), 8430.

(55) Brauer, B.; Chaban, G. M.; Gerber, R. B. *Phys. Chem. Chem. Phys.* **2004**, *6*, 2543.

(56) Brauer, B.; Dubnikova, F.; Zeiri, Y.; Kosloff, R.; Gerber, R. B. *Spectrochim. Acta, Part A* **2008**, *71*, 1438.

(57) Pele, L.; Gerber, R. B. *J. Chem. Phys.* **2008**, *128*, 165105.

(58) Chaban, G. M.; Gerber, R. B. *Theor. Chem. Acc.* **2008**, *120*, 273.

(59) Carbonniere, Ph.; Dargelos, A.; Ciofini, I.; Adamo, C.; Pouchan, C. *Phys. Chem. Chem. Phys.* **2009**, *11*, 4375−84.

CT900179D